Analyst

ROYAL SOCIETY OF CHEMISTRY

PAPER

View Article Online
View Journal | View Issue

Cite this: *Analyst*, 2022, **147**, 2757

Cytidine-rich hydrogel as an electrochemical signal amplification strategy for microRNA detection†

Xinying Zhang,[a,b] Zhiwei Zhang,[a,b] Chujing Yang,[a,b] Ziheng Hu,[a,b,c] Yingying Chen [a,b] and Lingyan Feng *[a,b]

Signal amplification strategies increase the complexities of biosensors while improving the response signals. Herein, a novel electrochemical biosensor was developed based on a DNA hydrogel for sensitive analysis using microRNA-21 (miRNA-21) as a detection model. Poly C sequences combined with C–Ag(I)–C hydrogel formed a DNA hydrogel by the unique interaction between the cytosines and silver ions. Thus, with a three-way conjunction structure of DNA, this C–Ag(I)–C hydrogel was constructed as a novel biosensor for the detection of miRNAs. With the assistance of this hydrogel, numerous silver ions gathered around DNA strands, which would amplify the signal. Under these conditions, the silver ions produced distinct square wave voltammetry oxidation peak currents. This electrochemical biosensor we designed exhibited a great linear relationship for the logarithm of the concentration of miRNA-21 from 1 fM to 100 pM with a detection limit of 0.117 fM. Furthermore, our sensors were able to differentiate miRNA-21 from its homologous family with satisfactory responsiveness in the dilute bovine serum system.

Received 19th April 2022,
Accepted 4th May 2022

DOI: 10.1039/d2an00667g

rsc.li/analyst

Introduction

MicroRNAs (miRNAs) are small single strands of noncoding RNAs that are inextricably linked to gene expression during virtually every cellular process.[1] As an example, microRNA-21 (miRNA-21) is a very important biomarker that is related to many types of cancers, such as brain cancer and lung cancer.[2] However, miRNAs are only 0.01% of the total RNA group, and the detection process has to be able to function in highly complex media.[3] Additionally, miRNAs are short and very unstable, which also increases the difficulty of obtaining accurate measurements. Therefore, ultrasensitive and selective detection for miRNAs is necessary for research purposes.

Various signal amplification strategies have been used in biosensors to achieve ultrasensitive detection. Hybrid chain reaction (HCR) and polymerase chain reaction (PCR) rolling circle amplification (RCA) are widely used in signal amplification.[4–6] Dirks and Pierce first used the HCR for signal amplification in 2004. As a type of isothermal and enzyme-free DNA signal amplification, HCR normally includes DNA hairpins with sticky ends and an initiator, which enables high selectivity of biosensors with the assistance of the Watson–Crick base-pairing rule. However, the drawbacks of HCR are also obvious.

Designing the DNA sequence used in HCR is very difficult as a result of unknown mechanisms operating in HCR. Compared with the HCR, the PCR strategy uses polymerase to synthesize a large number of nucleic acids that are used to form a number of complex structures. Although the isothermal enzyme polymerization reaction circumvented the requirement of high temperature for PCR, the usage of enzyme can still create numerous problems, such as the strict pH requirement and waste of nucleotides.[7] RCA can provide a large amount of oligonucleic acid structures that will greatly increase the sensitivity of biosensors.[8] Additionally, DNA machines are used in the amplification. DNA walkers walk on the surface of biosensors driven by the HCR or the DNA enzyme reaction.[9] Those strategies effectively increase the sensitivity of the biosensors. However, they also increase the difficulty of building biosensors with complex structures and repeated steps, and increase the cost of producing the biosensors due to the expensive enzymes.

DNA hydrogels have widely been used in recent years for constructing electrochemical biosensors because of their huge loading ability and satisfactory biocompatibility that can

[a]*Department of Materials Genome Institute, and Department of Chemistry, College of Science, Shanghai University, 200444 Shanghai, China. E-mail: lingyanfeng@t.shu.edu.cn*
[b]*Shanghai Engineering Research Center of Organ Repair, China*
[c]*Institute of Biological Information Processing, (IBI-3), Forschungszentrum Jülich GmbH, 52428 Jülich, Germany*

† Electronic supplementary information (ESI) available. See DOI: https://doi.org/10.1039/d2an00667g

provide signal probes and amplification strategies.[10,11] Typically, there are two types of DNA hydrogels: pure DNA hydrogels and hybrid DNA hydrogels used in biosensor construction.[12] Their use as biosensors is limited due to slow mass transfer of large molecules that block rapid detection,[13] and because complex strategies are used in building DNA hydrogel biosensors. There are numerous methods for building signal probes, such as chemical modification,[14] physical assemblies,[15] and loading cages.[11]

It was found that nucleotides can form hydrogels with the assistance of small molecules and ions. The construction of nucleotide hydrogels is simple, and they possess a wide variety of abilities.[16] The GMP hydrogel can increase the catalysis performed by hemin and is widely used to construct biosensors due to its catalytic ability and high loading capacity.[17,18] In 2019, it was observed the cytidine formed a new type of hydrogel that exhibited antibacterial activities. Cytidine combines with silver ions to form a C–Ag–C structure,[19] and thus the C–Ag(I)–C hydrogel contains many silver ions that can act as electrochemical signal probes. When silver ions were combined with the poly C sequence using a unique interaction between the cytosines and the Ag^{+}, a new type of DNA hydrogel was formed. Thus, there are two advantages to this DNA hydrogel. As a signal probe, it can simplify the building process of biosensors, and it can also provide a much higher electrochemical response that can be harnessed to design selective biosensors.

A DNA three-way junction (TWJ) is a unique branch structure that enables the modification of materials, and provides high selectivity and specificity. Moreover, due to the relaxed requirements for nucleic acid length, the TWJ structure can be combined with various amplification strategies.[20] In addition, locked nucleic acid (LNA) possesses a unique type of nucleotide sequence, whose 2′-o and 4′-c on the ribose is linked by methylene bridges, and this greatly increases the thermal stability of the LNA and the nucleic acid structures constructed by LNA.[21]

In this study, we combined DNA strands with a cytidine hydrogel to construct a simple sensitive electrochemical biosensor. We employed the C–Ag(I)–C hydrogel as the signal probe and used the signal amplification method. In the presence of miRNAs, the signal probe, which was the C–Ag(I)–C hydrogel that was constructed using a large amount of silver ions, was firmly modified on gold electrodes with the assistance of a DNA TWJ based on LNA in order to achieve sensitive and selective detection of miRNA-21 (Scheme 1).

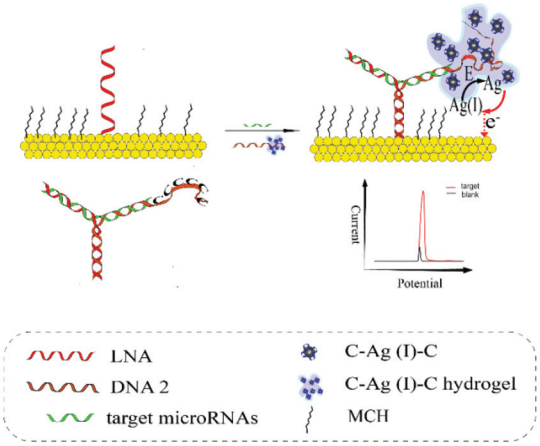

Scheme 1 Illustration of the electrochemical detection of miRNAs.

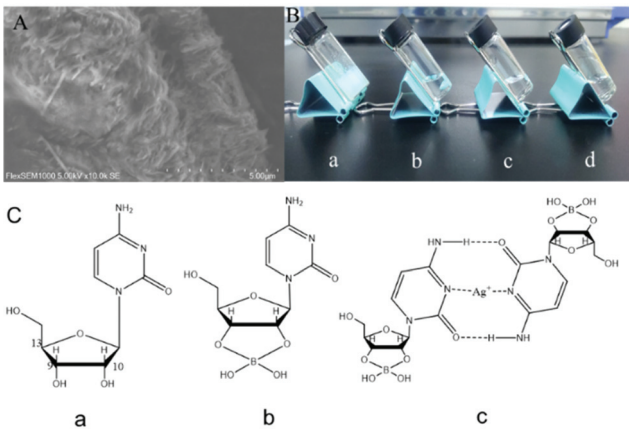

Fig. 1 The characterization of the C–Ag(I)–C hydrogel. (A) The SEM image of the C–Ag(I)–C hydrogel. (B) A photograph of the (a) C–Ag(I)–C hydrogel (500 mM 1 mL cytidine, 500 mM 500 μL silver ions, and 500 mM 1 mL boric acid), (b) the mixture of 500 mM 500 μL silver ions and 500 mM 1 mL cytidine, (c) the mixture of 500 mM 500 μL silver ions and 500 mM 1 mL boric acid, and (d) the mixture of 500 mM 1 mL cytidines and 500 mM 1 mL boric acid. (C) The chemical structure of the C–Ag(I)–C hydrogel: (a) the chemical structure of cytidines and (b) the chemical binding structure of boric acid and cytidines; (c) the chemical structure of the C–Ag(I)–C complex.

Results and discussion

The microstructure of the C–Ag(I)–C hydrogel, which was formed by the fiber-like structure of the C–Ag(I)–C complex, was measured by scanning electron microscope, as shown in Fig. 1A. A stable and insoluble hydrogel is shown in Fig. 1B in the photograph of different mixtures of the silver ions, cytidine, and boric acid. Obviously, the C–Ag(I)–C hydrogel was successfully constructed from the mixture of three elements (a), while the mixture of any other two elements: silver ions and cytidines (b), silver ions and boric acids (c), and cytidines and boric acids (d), did not result in any changes in the solution. This indicates that the silver ions, cytidine, and boric acid were all the elements necessary for the formation of the C–Ag(I)–C hydrogel.

As shown in Fig. 1C, boric acid acted as the linker for the structure formed by cytidine and silver ions *via* the interaction between the hydroxy of boric acid and the 9′-OH and 13′-OH in cytidine (b). The peak of the IR spectra at 1084 cm^{-1} was due to the formation of C–O–B bonds, which was the proof of the interaction of B–O–C (Fig. S3†). Therefore, these three

elements would combine together by the formation of C–Ag(I)–C (c). The XPS spectra of N 1s in Fig. S1† shows a peak at 398.6 eV because of the bonds of the C–Ag(I)–C structure. In this way, the C–Ag(I)–C units were connected one by one by boric acid to form a complex. Large amounts of silver ions were included in the formation of the C–Ag(I)–C hydrogel.

Circular dichroism (CD) spectra were used to confirm the construction of a three-way conjunction (Fig. S3†). When single-stranded DNA becomes double-stranded, there is hydrogen bond interaction between the bases to form the B structures that exhibit chiral enhancement, while the three-way conjunction structures formed by three single DNA strands are more rigid. Therefore, compared with single- and double-stranded DNA, the chirality in the TWJ structures is more optimal. There was a distinct increase in the positive peak at 275 nm that coincided with the appearance of the TWJ, which suggested that a tight B DNA structure formed.[22]

The process of construction of biosensors was confirmed by the cyclic voltammetry and AC impedance methods, using the $[Fe\ (CN)6]^{3-/4}$ couple as the electrochemical redox probe. As shown in Fig. 2A, the bare gold electrodes exhibited a reversible electro-redox reaction (a) whose redox separation performed closely to 56 mV, which was the standard value of the $[Fe\ (CN)_6]^{3-/4-}$. When the LNA modified it by Au–S bonds, the peak current slightly decreased (b) from 0.09 mA to 0.05 mA as a result of the blocking efficiency of LNA for the reaction of redox probes on the electrodes. Then, the modification of 6-mercaptohexanol (MCH) on the electrode surface led to the much lower peak current, and the redox potential was far removed from the common redox peak of $[Fe\ (CN)_6]^{3-/4-}$ (c), which was caused by the negative charge of MCH that was blocking the electronic transformation between the electrodes and the $[Fe\ (CN)_6]^{3-/4-}$ after MCH occupied the remaining reaction sites in order to avoid nonspecific absorption.

When the C–Ag(I)–C hydrogel was introduced on the modified electrodes, the peak current returned to 0.09 mA due to the excellent conductivity of the silver ions (d). The same result was obtained in the EIS investigation. A semicircle under high frequency was observed for the Nyquist plots, which was mainly constructed by the charge transfer resistance (R_{ct}) and the double-layer capacitance (C_{dl}) on the gold electrode surface, and a straight line at the low frequency domain using 5 mM $[Fe\ (CN)_6]^{3-/4-}$ as the signal probe. The R_{ct} of LNA-modified gold electrodes was slightly increased compared with the bare gold electrodes, whose R_{ct} was 61 Ω, as measured by the Autolab. After the modification of MCH, the R_{ct} of the electrodes (595 Ω) dramatically increased because of the increased hindrance and electrostatic repulsive interaction. Then, the C–Ag(I)–C hydrogel contained the target miRNA-21, and DNA 2 was modified on the surface of the work electrode, which caused the R_{ct} to decrease from 595 Ω to 356 Ω because of the excellent electroconductivity of silver ions. Thus, the successful construction of electrochemical biosensors was proven.

The EIS response of a three-way junction-modified gold electrode is shown in Fig. S4† to prove the successful construction of the TWJ structure on the surface of the gold electrodes. Compared with curve c in Fig. S4,† the gold electrodes modified by the TWJ structure were slightly higher as a result of increased electrostatic repulsion between the negatively charged phosphoric acid backbone and $[Fe\ (CN)_6]^{3-/4-}$. Under these conditions, the TWJ structure was successfully constructed on the gold electrodes.

To confirm that the cytidines can bind to the C sequence of DNA 2 with the assistance of the silver ions, we designed DNA strands whose sequences were the same as the DNA 2 but without the poly C sequence (DNA 0), and a DNA sequence with six cytidines at the 5′ end of DNA 1 (Table 1).

Fig. 3A shows the peak currents of the biosensors constructed by DNA 0, DNA 1, and DNA 2. Compared with the DNA strands without the C-rich sequences (DNA 0), the electrochemical biosensor, which was constructed by the DNA

Table 1 The sequences of oligonucleotides

Name	Sequences (5′–3′)
microRNA-21	UAGCUUAUCAGACUCGAUGUUGA
DNA 0	TCAACATCAGTTTTTTT
DNA 1	CCCCCCTCAACATCAGTTTTTTT
DNA 2	CCCCCCCCCCCCTCAACATCAGTTTTTTT
LNA	AAAAAACTGATAAGCTA-$(CH_2)_6$-SH

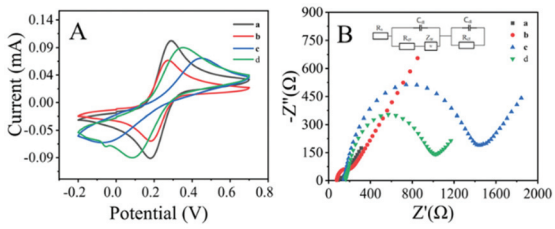

Fig. 2 The CV and EIS response of biosensors with different construction. (A) The CV and (B) EIS response of (a) the bare gold electrode, (b) the gold electrode stepwise-modified by LNA, (c) MCH, and (d) the C–Ag(I)–C hydrogel.

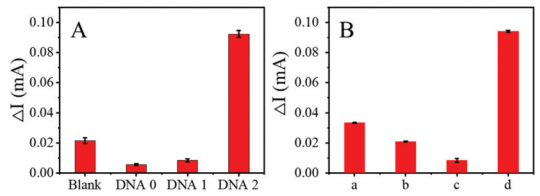

Fig. 3 The SWV response of different modifications of this biosensor. (A) The peak currents of the biosensors constructed by the DNA sequence without the C (DNA 0), the DNA sequence containing 6 cytidine bases (DNA 1), and the DNA sequence with 12 continuous cytidine bases (DNA 2). (B) The peak currents of the biosensor constructed by the mixture of (a) 60 mM $B(OH)_3$ and 60 mM $AgNO_3$ or (b) 60 mM cytidine and 60 mM $AgNO_3$; (c) 60 mM $AgNO_3$; and (d) the C–Ag(I)–C hydrogel.

designed with 12 C (DNA 2), provided nearly 8 times higher peak currents. Additionally, the peak current of the biosensor constructed by DNA 0 was similar to the peak currents of the biosensor in the absence of miRNA-21 (blank). In this process, the C–Ag(I)–C hydrogel was connected with the C sequence of DNA2 by the interaction of cytidines and silver ions to form the C–Ag(I)–C hydrogel, which loaded very large amounts of silver ions to produce much higher currents. However, the peak currents produced by the biosensor made by DNA 1, which contained six C at the 5′ end and was shorter than DNA 2, were slightly higher than the signal produced by DNA 0, which did not have cytidines at the end of the 5′ sequences.

The peak currents of the biosensor made by DNA 2 were nearly 8 times those of the biosensor made by DNA 1. Therefore, there was no positive correlation between the length of the C sequence and the peak currents, which proved that there was a unique combination between the C–Ag(I)–C hydrogel and the C-rich sequence of DNA 2. The reason for this was because of the weak non-covalent interaction between silver ions and cytosines. DNA 1 contained six cytosines, and cannot provide a stable interaction with the C–Ag(I)–C hydrogel. Therefore, the C–Ag(I)–C hydrogel provided the signal probes for this biosensor and proved that modification of the C–Ag(I)–C hydrogel by DNA 2 occurred without any covalent interaction. It was available for the modification of the C–Ag(I)–C hydrogel.

To demonstrate the hydrogel signal amplification capacity, it was measured for different combinations of the three components constituting the hydrogel. In Fig. 3B, the peak currents of the biosensors formed by (a) the mixture of boric acid and silver nitrate, (b) the mixture of cytidine and silver nitrate, and (c) pure silver nitrate were measured under the same conditions. The peak currents produced by (c) pure silver nitrate were much lower compared with the (d) C–Ag(I)–C hydrogel, which were close to one in ten and thus proved the signal amplification strategy. The C–Ag(I)–C hydrogel provided silver ions far beyond the amount absorbed on the DNA structure by electrostatic adsorption and the non-covalent interrelation between the silver ions and cytidine for the biosensors.

Compared with the biosensors produced by the mixture of any two elements in the C–Ag(I)–C hydrogel, the biosensor constructed by the C–Ag(I)–C hydrogel exhibited much higher peak current. Thus, the formation of the C–Ag(I)–C hydrogel was very important for signal amplification. Boric acid drove the orderly repeated accumulation of the C–Ag(I)–C structure, which provided a stable structure for this hydrogel. The surface modification density is the key factor that affects the appearance of the electrochemical biosensors. Therefore, the concentration of LNA, which was the capture probe, was optimized to 4 nM (Fig. S5†).

Based on the combination of the C–Ag(I)–C hydrogel and the TWJ structure, a biosensor for miRNA-21 was successfully constructed. Subsequently, the currents at different concentrations of miRNA-21 were recorded (Fig. 4A). The peak currents of the biosensor generally increased following the increase in the concentration of miRNA-21, because the

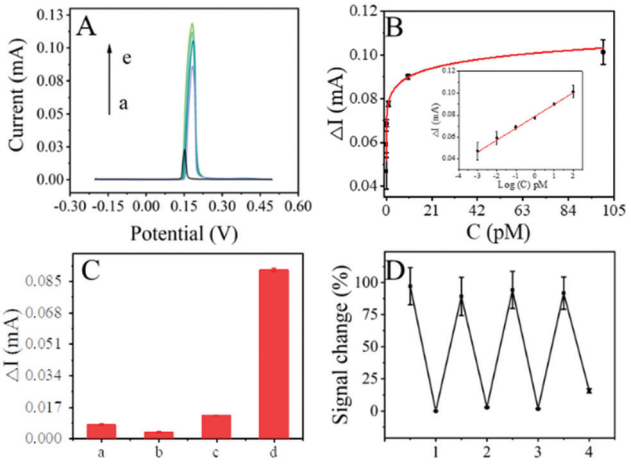

Fig. 4 The performance of the biosensor. (A) SWV response and (B) peak current intensities in the presence of different miRNA-21 concentrations from (a) 0 fM to (e) 100 pM. The linear relationship between SWV peaks and the logarithm of the miRNA-21 concentration is shown in the inset. (C) The selectivity of the sensor hybridized to different miRNA sequences: (a) single-base mismatched miRNA-21; (b) three-base mismatched miRNA-21; (c) noncomplementary miRNA-21; and (d) miRNA-21. (D) The recovery of the biosensor.

increased formation of TWJ structures resulted in a larger C–Ag(I)–C hydrogel that was able to gather additional Ag^+ in this skeleton on the gold electrodes. Fig. 4B shows the relationship between the concentration of miRNA-21 and the square wave voltammetry (SWV) responsive currents. As shown in the figure insert in Fig. 4B, there was a satisfactory linear relationship between the current and the logarithmic concentration of miRNA-21 in the range of 1 fM to 100 pM, with a detection limit of 117 aM (S/N = 3).

The linear relationship can be represented as $\Delta I = 0.01085 \log c + 0.07874$, with a correlation coefficient of 0.996 ($\Delta I = I - I_0$ I: the peak current of this biosensor in the presence of target miRNA-21; I_0: the peak current of this biosensor without target miRNA-21). This result proved that the biosensor we designed had the ability to detect miRNAs with ultrasensitivity. Selectivity was another factor used to evaluate biosensors. Thus, we employed miRNA-21 and created a mismatch of (a) one base chain, (b) three base chains, and (c) non-complementary chains to experience the process of construction of our biosensor. The selectivity of the biosensor was determined in Fig. 4C. Compared with the signal of (a) single mismatch miRNA-21, (b) triple mismatch miRNA-21, and (c) non-complementary miRNA-21, whose concentration was 10 pM, the signal that was produced by the target miRNA-21 was the highest. It was approximately the fourth case for different mismatches with miRNA-21. Thus, the biosensor we designed exhibited excellent specificity.

The regeneration of the biosensor is shown in Fig. 4D. The hydrogen bond formed by the double DNA strands can be destroyed by guanidine hydrochloride. Therefore, we used it to destroy the secondary structure of the three-way conjunction we designed in order to measure the regeneration of our bio-

sensor. This sensor exhibited satisfactory recovery for the 100% signal reconstruction during the second test, and the recoveries for the third and fourth test were nearly 100%.

To test the proposed biosensor for detection of miRNA in a real environment, the marker recovery method was used in our work. The SWV tests for this biosensor were prepared in a solution of a defined amount of target miRNA, which was dissolved in bovine serum samples that were diluted 100 times with PB buffer (pH 7.0 20 mM). Recovery of this biosensor was calculated in Table S2,† and it ranged from 97.7% to 108.6%, which confirmed the great usage possibilities for this biosensor with real samples. The relative standard deviation (RSD) values were less than 10%. The biosensor we designed showed excellent detection capability when real samples were used, as shown in Table S2.† When compared with other works (Table S1†), the electrochemical biosensor possessed the characteristics of simpler construction, wider linear range, and lower detection limit that reached 117 aM.

Experimental

Reagents and materials

Cytidine and boric acid were purchased from Aladdin Reagents. Silver nitrate ($AgNO_3$) was obtained from Shanghai No. 1 Reagent Factory. 6-Mercaptohexanol (MCH), the HPLC-purified DNA2 and LNA, and miRNA-21 were synthesized by Sangon Biotech Co. (Shanghai, China). The sequences of these oligonucleotides are shown in Table 1. All reagents were used without any purification. All the solutions were prepared using ultrapure water (18.2 MΩ, Milli-Q, Millipore) in order to avoid the influence of anions that could combine with the silver ions to form insoluble salts. Bovine serum was obtained from the Sangon Biotech Co. (Shanghai, China).

Instruments

A traditional three-electrode system was used for all electrochemical measurements: modified gold electrodes (1 mm in diameter) were used as the work electrodes, the counter electrodes were platinum wire electrodes, and the reference electrodes were saturated calomel electrodes. The square wave voltammetry and cyclic voltammetry were performed with an Autolab potentiostat/galvanostat instrument (Metrohm China Ltd, Switzerland). Circular dichroism was measured on a JASCO-1500 instrument (Japan).

Preparation of the gold electrodes

The gold electrodes used in our experiments were polished with 0.3 Polish power for 1 minute. Then, they were polished with a 0.05 mm polished plate for 5 minutes. Finally, the electrodes were ultrasonically cleaned with water and ethanol for two minutes each time. The electrodes were polished by electrochemical cleaning using the three-electrode system under 0.5 M NaOH and 0.5 M H_2SO_4, 0.1 M H_2SO_4/0.01 M KCl, and 0.05 M H_2SO_4.

Synthesis of the C–Ag(I)–C hydrogel

For synthesis, 3 μL 60 mM cytidine and 3 μL 4 nM DNA 2, and then 1.5 μL 60 mM $AgNO_3$ and 3 μL 60 mM $B(OH)_3$ were mixed together step by step following oscillation at room temperature. This 10.5 μL mixture was reacted at room temperature for 1 hour in the dark to form the C–Ag(I)–C hydrogel. Then, the mixture was coated onto the surface of modified gold electrodes for further use.

Modification of the gold electrodes

A mixture of 3 μL 100 nM tris(2-carboxyethyl)phosphine (TCEP) and 3 μL 4 nM LNA was dripped onto the surface of gold electrodes, which were cleaned in the first step. Next, the modified electrodes equilibrated at room temperature overnight in order to fabricate the LNA strands bound to the gold electrodes by Au–S binding. Following that, 6 μL 100 nM MCH was dripped onto the electrodes, which had been immersed in ultrapure water for 1 minute and then dried. In this procedure, MCH would block the LNA unoccupied binding sites on the modified electrodes in order to decrease the non-specific absorbance.

Construction of the three-way junction

After mixing with 3 μL of different concentrations of MIR-21 (the instruments used in this step were treated with high-temperature sterilization), the hydrogel was attached to the electrodes, whose surfaces were totally modified with LNA. Then, the electrodes with the hydrogel were incubated at 37 °C for 2 hours in order to form the TWJ structure. Finally, the electrodes modified with the hydrogel were immersed in ultrapure water for 30 seconds to remove nonspecific absorption.

Detection of the biosensor

The signal responses of the biosensor *via* square wave voltammetry (SWV) were measured in 0.1 M KCl solution. The parameters used for the SWV method were a duration time of 1 min, and a frequency of 25 Hz. The oxidation peak occurred at approximately 0.18 V.

Conclusions

We developed a novel DNA hydrogel for the sensitive detection of miRNAs. The C–Ag(I)–C hydrogel was constructed by simply mixing the reactants together to simplify the steps of the biosensor construction. It was specifically combined with DNA 2, which could connect with miRNA-21 and form the TWJ structure. In this way, the huge amount of silver ions, which functioned as the signal probe, included in the C–Ag(I)–C hydrogel provided eight times higher peak current than the blank and ten times higher peak current than the current produced by the simple connection between Ag^+ and C. The C–Ag(I)–C hydrogel combined with the formation of a TWJ structure achieved the goals of signal amplification and high selectivity.

Under the optimal state, the established method revealed satisfactory sensitivity and excellent selectivity. The detection

limit was 117 aM, which meets the requirements of early cancer detection. More profoundly, there are excellent prospects for practical applications of this electrochemical DNA biosensor. There was no obvious influence on the biosensor by the diluted bovine serum. With its simple construction, it could serve as a simple and general electrochemical biosensor for the detection of miRNAs.

Conflicts of interest

There are no conflicts to declare.

Acknowledgements

This work was funded by the National Natural Science Foundation of China (No. 21705106) and the National Science Foundation of China (No. 22177067); the Program for Professor of Special Appointment (Eastern Scholar) at Shanghai Institutions of Higher Learning (No. TP2016023); the Shanghai Natural Science Foundation (No. 18ZR1415400); and the Shanghai Sailing Program (No. 20YF1413000).

Notes and references

1 V. Ambros, Mathematics of microRNAs: stabilizing gene regulatory networks, *Natl. Sci. Rev.*, 2019, **6**(6), 1189–1190.
2 D. Bautista-Sanchez, C. Arriaga-Canon, A. Pedroza-Torres, I. A. De La Rosa-Velazquez, R. Gonzalez-Barrios, L. Contreras-Espinosa, R. Montiel-Manriquez, C. Castro-Hernandez, V. Fragoso-Ontiveros, R. M. Alvarez-Gomez and L. A. Herrera, The Promising Role of miR-21 as a Cancer Biomarker and Its Importance in RNA-Based Therapeutics, *Mol. Ther.–Nucleic Acids*, 2020, **20**, 409–420.
3 T. Jet, G. Gines, Y. Rondelez and V. Taly, Advances in multiplexed techniques for the detection and quantification of microRNAs, *Chem. Soc. Rev.*, 2021, **50**(6), 4141–4161.
4 K. Zhang, S. Lv, Q. Zhou and D. Tang, CoOOH nanosheets-coated g-C3N4/CuInS2 nanohybrids for photoelectrochemical biosensor of carcinoembryonic antigen coupling hybridization chain reaction with etching reaction, *Sens. Actuators, B*, 2020, **307**, 127631.
5 Z. Li, H. Xu, S. Li, S. Wu and X. Miao, Zettomole electrochemical HIV DNA detection using 2D DNA-Au nanowire structure, hemin/G-quadruplex and polymerase chain reaction multi-signal synergistic amplification, *Anal. Chim. Acta*, 2021, **1159**, 338428.
6 K. Zhang, S. Lv, Z. Lin, M. Li and D. Tang, Bio-bar-code-based photoelectrochemical immunoassay for sensitive detection of prostate-specific antigen using rolling circle amplification and enzymatic biocatalytic precipitation, *Biosens. Bioelectron.*, 2018, **101**, 159–166.
7 T. Kilic, A. Erdem, M. Ozsoz and S. Carrara, microRNA biosensors: Opportunities and challenges among conventional and commercially available techniques, *Biosens. Bioelectron.*, 2018, **99**, 525–546.
8 R. Abolhasan, A. Mehdizadeh, M. R. Rashidi, L. Aghebati-Maleki and M. Yousefi, Application of hairpin DNA-based biosensors with various signal amplification strategies in clinical diagnosis, *Biosens. Bioelectron.*, 2019, **129**, 164–174.
9 Y. H. Wang, W. Song, H. Y. Zhao, X. Ma, S. Y. Yang, X. J. Qiao, Q. L. Sheng and T. L. Yue, DNA walker-assisted aptasensor for highly sensitive determination of Ochratoxin A, *Biosens. Bioelectron.*, 2021, **182**, 7.
10 K. Zhang, M. Pei, Y. Y. Cheng, Z. Zhang, C. Niu, X. Q. Liu, J. X. Liu, F. Guo, H. G. Huang and X. J. Lin, A novel electrochemical aptamer biosensor based on tetrahedral DNA nanostructures and catalytic hairpin assembly for CEA detection, *J. Electroanal. Chem.*, 2021, **898**, 8.
11 Y. N. Hou, R. Han, Y. L. Sun, C. N. Luo and X. Y. Wang, Chemiluminescence sensing of adenosine using DNA cross-linked hydrogel-capped magnetic mesoporous silica nanoparticles, *Anal. Chim. Acta*, 2022, **1195**, 9.
12 S. Iqbal, F. Ahmed and H. Xiong, Responsive-DNA hydrogel based intelligent materials: Preparation and applications, *Chem. Eng. J.*, 2021, **420**(Part 3), 130384.
13 M. Chen, Y. Wang, J. Zhang, Y. Peng, S. Li, D. Han, S. Ren, K. Qin, S. Li and Z. Gao, Stimuli-responsive DNA-based hydrogels for biosensing applications, *J. Nanobiotechnol.*, 2022, **20**(1), 40.
14 S. Liu, W. Su, Y. Li, L. Zhang and X. Ding, Manufacturing of an electrochemical biosensing platform based on hybrid DNA hydrogel: Taking lung cancer-specific miR-21 as an example, *Biosens. Bioelectron.*, 2018, **103**, 1–5.
15 X. Mao, D. Mao, T. Chen, M. Jalalah, M. S. Al-Assiri, F. A. Harraz, X. Zhu and G. Li, DNA Hydrogel-Based Three-Dimensional Electron Transporter and Its Application in Electrochemical Biosensing, *ACS Appl. Mater. Interfaces*, 2020, **12**(33), 36851–36859.
16 H. Wang, X. Q. Xie, Y. Peng, J. Li and C. S. Liu, ., Self-healing mechanism and bioelectrochemical interface properties of core-shell guanosine-borate hydrogels, *J. Colloid Interface Sci.*, 2021, **590**, 103–113.
17 J. Ye, L. P. Zhu, M. X. Yan, T. Xiao, L. B. Fan, Y. Xue, J. S. Huang and X. R. Yang, An intensive and glow-type chemiluminescence of luminol-embedded, guanosine-derived hydrogel, *Talanta*, 2021, **230**, 7.
18 R. Zhong, Q. Tang, S. Wang, H. Zhang, F. Zhang, M. Xiao, T. Man, X. Qu, L. Li, W. Zhang and H. Pei, Self-Assembly of Enzyme-Like Nanofibrous G-Molecular Hydrogel for Printed Flexible Electrochemical Sensors, *Adv. Mater.*, 2018, **30**(12), e1706887.
19 Q. Tang, T. N. Plank, T. Zhu, H. Yu, Z. Ge, Q. Li, L. Li, J. T. Davis and H. Pei, Self-Assembly of Metallo-Nucleoside Hydrogels for Injectable Materials That Promote Wound Closure, *ACS Appl. Mater. Interfaces*, 2019, **11**(22), 19743–19750.
20 J. Moon, J. Lim, S. Lee, H. Y. Son, H. W. Rho, H. Kim, H. Kang, J. Jeong, E. K. Lim, J. Jung, Y. M. Huh, H. G. Park

and T. Kang, Urinary exosomal mRNA detection using novel isothermal gene amplification method based on three-way junction. Biosens, *Bioelectronics*, 2020, **167**, 8.

21 X. J. Piao, H. Z. Wang, D. W. Binzel and P. X. Guo, Assessment and comparison of thermal stability of phosphorothioate-DNA, DNA, RNA, 2 '-F RNA, and LNA in the context of Phi29 pRNA 3WJ, *RNA*, 2018, **24**(1), 67–76.

22 J. Kypr, I. Kejnovska, D. Renciuk and M. Vorlickova, Circular dichroism and conformational polymorphism of DNA, *Nucleic Acids Res.*, 2009, **37**(6), 1713–1725.